Cavity-Enhanced Frequency Modulation Spectroscopy: Advancing Optical Detection Sensitivity and Laser Frequency Stabilization

Jun Ye,[†] Long-Sheng Ma,[☞] and John L. Hall[‡]
JILA, University of Colorado and National Institute of Standards and Technology
Boulder, Colorado 80309-0440

ABSTRACT

High detection sensitivities of quantum absorptions are important in many research fields of physics, chemistry and biology. In this paper we present our latest results on the ultrasensitive molecular overtone spectroscopy using the cavity-enhanced frequency modulation (FM) technique. The principle of this method makes use of a high-finesse external cavity to enhance the intrinsic resonance contrast, while an FM modulation approach provides shot-noise limited signal recovery. Ideal matching of the FM sideband frequency to the cavity free-spectral-range makes the detection process insensitive to the laser frequency noise relative to the cavity, while at the same time overcomes the cavity bandwidth limit. Working with a 1064-nm Nd:YAG laser, we have obtained sub-Doppler overtone resonances of HCCD, HCCH and CO_2 molecules. A detection sensitivity of 5×10^{-13} of integrated absorption (1×10^{-14} / cm) over 1-s averaging time has been achieved. The resultant high signal-to-noise ratio of the weak resonance produces excellent laser frequency stabilization.

Keywords: FM spectroscopy, Cavity enhancement, Ultrasensitive detection, Optical frequency standards

1. Introduction

The continuing quest for higher-quality frequency standards has led to rapid progresses in high-resolution spectroscopy. Narrow atomic resonances are of primary interest, owing to the strong intrinsic correlation between resonance linewidth and the obtainable stability/reproducibility of the associated standard. Great efforts have been invested in order to separate the resonance information itself from the inevitable background, in terms of both the favorable alteration of the basic interaction process between the matter and light, for example the reduction of the second order Doppler effect, and the judicious design of signal encoding (modulation) and decoding (demodulation) schemes. The abundance of environmentally insensitive and stable molecular ro-vibrational transitions make them a natural choice for optical frequency standards, with the typical resonance linewidth on the order of kHz. However, to cover the visible part of the optical spectrum we have to resort to the vibration-overtone transitions, which can be easily a million times weaker than their fundamental counterparts. Detection sensitivities are thus seriously demanding, as the recovered signal-to-noise ratios (S/N) translate directly to the short-term stability of the standard, or its conjugate, the length of the averaging time one has to wait to achieve a certain accuracy. This scientific exploration was our initial motivation behind the development of the cavity-enhanced frequency modulation (FM) spectroscopy described in detail hereinafter. The result of this new spectroscopic technique is the much enhanced detection sensitivity of the order of 10^{-12} integrated absorption, which has yielded - even with the weak overtone transitions - spectacular optical frequency stabilities previously achieved only with the electronic resonance of iodine molecules (~ a million times stronger absorption than the overtones we used).

Sensitive detections are of course desired in other branches of science as well. Indeed, the unprecedented sensitivity reported here should open the door for many other useful applications. Combined with resolution, high sensitivity has often been the leading force in discovering new physical processes and in testing fundamental physical postulates. Many interesting molecular dynamics can be studied, including the highly excited vibration-overtone modes which could display permutation splittings associated with exchange of atoms. On the practical side, one can easily envision the optimized use of high sensitivity in the trace gas monitoring and sensing.

2. Optical Detection Sensitivity: Fundamental Limit

Ultrasensitive detection of optical absorption by atomic/molecular samples can be facilitated by either enhancing the intrinsic absorption signal (contrast) or reducing the background noise, ideally to the fundamental quantum limit. In this section we will concentrate on the noise aspect. The ultimate detection sensitivity is achieved when we are able to observe each

absorption event, with the noise basically limited by the uncertainty of event occurrence, namely the shot noise in the signal. From here we understand the shot noise is associated with the discrete nature of the interaction process between matter and photon streams obeying certain (Poissonian) statistics. The shot noise is fundamental in that it reflects the quantum nature of light. (Methods to circumvent this noise limit are not discussed in this paper.) Beer's absorption law states that light passing through an atomic/molecular sample of length L will be attenuated by the factor $e^{-\alpha \cdot L}$. The physical origin of this attenuation process is due to the destructive interference between the incident radiation and the electric field generated by the coherently-driven sample dipole moments.[1] Therefore the direct absorption is an intrinsically microscopic (quantum mechanical) effect. It can be viewed as homodyne detection as the two interfering fields have the same frequency. The maximum sensitivity condition will arise if the probe field has no amplitude noise beyond its intrinsic quantum fluctuation. Given a detection bandwidth of B, the minimum detectable absorption signal under this shot-noise limit is

$$ \left(\alpha L \right)_{min} = \left(\frac{2eB}{\eta P_0} \right)^{1/2} , \tag{1} $$

where e is the electron charge, η is the photodetector responsivity in Amp/Watt, and P_0 is the incident radiation power. This sensitivity can be as high as 2×10^{-8} of integrated absorption at 1 s averaging for $P_0 = 1$ mW and a reasonable η (~ 0.8 Amps/Watt at 1.064 μm). In practice, however, noises of various technical origins tend to become dominant in the low frequency ranges. A noisy background severely impacts the measurement of a small change of signal, with the resultant S/N being several orders of magnitude worse than the shot noise limit. In order to avoid excessive low-frequency noise of technical origins, one can use modulation techniques, either on the laser amplitude or frequency, to encode and then detect the absorption at a higher frequency and within a narrower bandwidth. Reduced-background detection techniques are also quite often used in avoiding excessive noises.

Signal detections employing ac methods permit comparisons of on-resonant and off-resonant cases in quick succession. By simultaneously obtaining and subtracting these cases, one provides a signal channel with no output unless there is a resonance. This is conveniently accomplished by using high-frequency modulation (FM) technique.[2,3] FM spectroscopy is one of the most powerful spectroscopic techniques available for super-sensitive and high-speed detections of weak absorption signals. In principle, FM spectroscopy offers a detection sensitivity approaching that of Equation (1), limited only by the fundamental quantum noise. A reasonable modulation index is needed to recover adequate signal size, however, compared with low-frequency modulation processes, the associated linewidth broadenings and lineshape distortions are not present in high-frequency FM. When scanning through resonance, the wide spread FM spectra allows each individual component to interact with the spectral features of interest and thereby preserves the ultrahigh resolution capability of contemporary narrow-linewidth lasers. The high bandwidth associated with the high-frequency modulation enables rapid signal recovery.

In FM spectroscopy the probing field is phase-modulated at a frequency much larger than the resonance linewidth under study. Subsequent heterodyne and rf phase-sensitive detection yield the desired signal. The high sensitivity associated with the FM spectroscopy is mainly due to its high modulation frequency, usually chosen to lie in a spectral region where the amplitude noise level of the laser source approaches the quantum (shot noise) limit. The redistribution of some of the carrier power to its FM sidebands causes only a slight penalty in the recovered signal size. When the modulation index β is on the order of unity or less, the FM spectrum can be approximated by a carrier (~ $J_0(\beta)$) and two first order sidebands (~ $J_1(\beta)$). Here J_0 (J_1) is the zero (first) order Bessel function. If only the carrier is tuned to interact with a narrow sub-Doppler resonance, then the detection process is intrinsically dispersion-sensitive. Assuming the total probe power is still P_0, the detected shot noise current is given by $\sqrt{2eB\eta P_0 \left(J_0^2 + 2J_1^2 \right)} \approx \sqrt{2eB\eta P_0}$, while the signal current arising from the heterodyne beat between the carrier and the sidebands becomes $\sqrt{2}\eta P_0 J_0 J_1 \cdot \phi$, with ϕ being the associated resonance phase shift. The magnitude relationship between dispersion and absorption ($\phi = \Delta n \cdot \omega L / c$ and $\Delta n = \alpha \cdot \lambda / 4\pi$, where n is the refractive index) sets the scale of the equivalent minimum absorption at the shot-noise limit,

$$ \left(\alpha L \right)_{min} = \left(\frac{2eB}{\eta P_0} \right)^{1/2} \frac{\sqrt{2}}{J_0(\beta) J_1(\beta)} . \tag{2} $$

The modulation-dependent function $J_0(\beta) J_1(\beta)$ has its maximum value of 0.34 at $\beta \approx 1.1$. Compared with Equation (1) for the ideal case of homodyne detection, FM heterodyne detection suffers a factor of ~ 4 loss in sensitivity for fixed total optical power. This is the (small) price for totally avoiding the laser's technical noise. It arises in part due to the power reduction implied in converting some of the main carrier to sidebands and in part from the down-conversion of shot noise from two

additional spectral windows by the two sidebands. Carefully designed FM detection can often nearly reach the sensitivity limit set in Equation (2). This sensitive nature of FM spectroscopy along with its high resolution and high speed detection capabilities have made this technique very popular.

3. Enhanced Sensitivity: The Use Of An Optical Resonator

After addressing the noise issue, we naturally have to turn our attention to the signal itself to further advance the detection sensitivity. An optical cavity placed around the absorber is an effective technique to enhance the absorption contrast, as conveniently explained in terms of extending the effective cell length. From another view-point, for a given noise generated by transmitted dc light on the detector, the high internal build-up field of the cavity elicits a strong molecular radiation, which is resonantly coupled out for detection. It was realized in the early days of laser development that a laser cavity can be used to greatly enhance the absorption detection sensitivity,[4] by taking advantage of the multi-pass effect and the delicate balance between the laser gain and intracavity absorption.[5,6] However, it is now often preferred to separate the absorber from the laser in order to extend the experimental flexibility and to have better controlled working parameters. Enhancement of absorption sensitivity has been accomplished by using long multi-pass absorption cells.[7] Kastler suggested a Fabry-Perot cavity could be used because its transmission is sensitive to small variations of its inside absorption.[8] For high-resolution, Cerez et al.[9] first applied this external cavity technique to saturated absorption spectroscopy. Ma and Hall[10] were able to use an external resonator combined with the optical heterodyne spectroscopy to achieve excellent signal-to-noise ratios. The use of an external cavity for the detection of molecular overtone transitions was also demonstrated later.[11] In linear-absorption experiments, an enhancement cavity has been used most extensively in the context of ring-down spectroscopy.[12]

The advantages of using an external optical resonator are manifold. First of all, the effective absorption length of the intracavity absorber is increased by a factor of $(2 \cdot \text{Finesse}/\pi)$. This directly increases the detection sensitivity. Secondly, the cavity builds up its intracavity power. This allows the use of low-power lasers for the input, even for the weak transitions which require large intensities to saturate. It also reduces the output power level that needs to be handled by a photodetector. In addition, the geometrical self-cleaning and matching of the two counter-propagating waves inside the cavity are important both for eliminating pointing-direction-related noises and for obtaining narrow and unshifted resonance lines, as explained by Hall and Bordé.[13] Furthermore, the same stable cavity can be used to pre-stabilize the laser frequency when it is locked on the cavity resonance, thereby reducing the detection noise.

In the following we define some relevant cavity parameters. The input coupling mirror has a power transmission coefficient of T_{in} and loss of L_{in}, while for the output coupler they are T_{out} and L_{out}, respectively. The total empty cavity loss $L_{cav} = T_{in} + T_{out} + L_{in} + L_{out}$. The input optical power is P_{in}, the cavity-reflected power is P_r, and the cavity-transmitted power is P_t. The cavity finesse (F) is simply

$$F = \frac{2\pi}{L_{cav}} \ .$$

(3)

The (resonant-) cavity reflection efficiency (R_{cav}), transmission efficiency (T_{cav}), and intracavity build-up power can be expressed as

$$\frac{P_r}{P_{in}} = R_{cav} = \left(L_{in} + L_{out} + T_{out} - T_{in} \right)^2 \left(\frac{1}{L_{cav}} \right)^2 \ ,$$

$$\frac{P_t}{P_{in}} = T_{cav} = 4 T_{in} T_{out} \left(\frac{1}{L_{cav}} \right)^2 \ ,$$

(4)

$$\frac{P_c}{P_{in}} = 4 T_{in} \left(\frac{1}{L_{cav}} \right)^2 \ .$$

Assume the cavity length is L and it is filled with a weakly-absorbing gas sample with an absorption coefficient of α per unit length. By weakly-absorbing we mean the cavity round trip loss due to the sample is: $1 - \exp(-2\alpha L) \approx 2\alpha L$. In a direct absorption measurement with a single-pass gas cell of length L, the output power is: $P_{out} = P_{in} \cdot e^{-\alpha L} \approx P_{in} (1 - \alpha L)$. Therefore the absorption signal is $P_{in} \cdot \alpha L$, while the shot noise is determined by the overall output power $P_{out} \approx P_{in}$, in the weak absorption limit. The noise-equivalent minimum absorption sensitivity is given by Equation (1).

When the sample is placed inside a cavity, the transmitted power is modified from Equation (4),

$$\frac{P_t}{P_{in}} = 4T_{in}T_{out}\left(\frac{1}{L_{cav}+2\alpha L}\right)^2 = \frac{4T_{in}T_{out}}{L_{cav}^2}\left(\frac{1}{1+\frac{2\alpha L}{L_{cav}}}\right)^2$$
$$\approx \frac{4T_{in}T_{out}}{L_{cav}^2}\left(1-2\frac{2\alpha L}{L_{cav}}\right).$$

(5)

The detected signal contrast in the cavity transmission is therefore enhanced,

$$\frac{\delta P_t}{P_t} = 2\frac{2\alpha L}{L_{cav}}$$
$$= \frac{2F}{\pi}\cdot(\alpha L)\ .$$

(6)

Considering shot-noise, the associated minimum detectable absorption is

$$(\alpha L)_{min} = \frac{\pi}{2F}\cdot\left(\frac{2eB}{\eta P_t}\right)^{1/2} = \frac{\pi}{2F}\cdot\left(\frac{2eB}{\eta T_{cav}P_{in}}\right)^{1/2}\ .$$

(7)

The mirror parameters can be pre-designed to maximize the resonant cavity transmission T_{cav}, by taking into consideration of the intracavity gas absorption.

It is clear from Eq. (4) that the intracavity circulating power can be much larger than the input power. This power buildup is useful in producing an appreciable level of saturation of very weak transitions for sub-Doppler resolution. The strong light field drives the molecular dipole moments in a phase-coherent fashion. The radiation from these prepared dipole moments is essentially the signal we want to detect. However, the strong background of the un-absorbed incoming light sets the detection shot noise level. With the buildup cavity, this large noise contribution is reduced after the sample has been prepared and before the final detection. When the cavity is tuned onto a molecular line, a major part (determined by the cavity efficiency) of the molecular signal will leak out of the cavity to reach a detector, while a similar (or smaller) portion of the input power will be transmitted by the cavity and reach the same detector to set the shot noise limit. The large intracavity buildup power, however, will remain trapped inside, after having phase-coherently prepared the molecular dipole moments. This result, although explained from a different but more fundamental angle, is intrinsically the same manifestation of the cavity enhancement effect, as discussed in the previous paragraphs.

From the technical side, another advantage of the cavity is also clear when the laser source has a relatively large amplitude noise. For shot-noise limited detection, the optimum intensity range tends to be pushed lower when there is a larger amplitude noise. Fortunately with the buildup cavity, the detector does not have to receive the large intensity. This effect is similar to the result of polarization spectroscopy[14] or interference filtering. Usually a reasonable power level of cavity transmission can be easily found to operate near or within the shot noise limited regime.

4. Principles of the Noise-Immune Cavity-Enhance Optical Heterodyne Molecular Spectroscopy

Equation (7) shows that a shot noise limited absorption sensitivity of $10^{-12} - 10^{-13}$ is in principle available, using an external enhancement cavity of finesse $\sim 10^5$, and about 1 mW of cavity transmitted power. The hard part is to find the appropriate signal recovery process such that we are indeed shot noise limited. Technical noises associated with the optical source and with the cavity instability need to be reduced or eliminated. It is clear some form of modulation technique will have to be used to encode the signal at a high frequency to avoid the low-frequency source noise while at the same time the rapidly-evolving time-dependent signal allows the effective subtraction of the background fluctuations caused by the cavity instability. This later point is important, as evidenced by the fact that no transit-domain ring-down spectroscopy has so far been able to approach the stated shot noise limit, even though the technical noise of light is effectively filtered out using cavity stored photons.

The first modulation approach which comes to mind is simply to lock the laser frequency tightly on the corresponding cavity resonance and then dither the cavity mode around the desired molecular resonance. The cavity transmission is

monitored. This approach is essentially a simple lock-in derivative-lineshape recovery process. In order for this method to be effective, it is important to have a super-tight frequency lock loop between the laser and the cavity since any laser frequency noise relative to the cavity will be converted to amplitude noise in detection. A piezo-electric transducer mounted on one of the cavity mirrors can be used to modulate the cavity length and the laser will track this modulation. The modulation frequency is usually limited to the audio range due to the mechanical resonance and roll-off of the PZT and mirror assembly. Depending upon the laser (amplitude) noise spectral distribution, the accessible modulation frequency may be too low to reach the shot-noise-limited spectral region. The intrinsic lineshape could also be modified (broadened) by this modulation process.

To enjoy the noise-reduction advantages of heterodyne spectroscopy, one needs to increase the phase-modulation frequency of the probing field, usually to be much larger than the resonance linewidth under study. Besides the laser-cavity locking issue, we are then faced with another obstacle, namely the cavity bandwidth limit. Too high a modulation frequency simply reduces the coupling of the sidebands into the cavity and thereby denies their useful interactions with molecules. For a cavity with a reasonable length, say 50 cm, and a finesse of 10,000, its linewidth (FWHM) is only 30 kHz. A modulation frequency this low seldom yields a shot-noise limited performance. What is needed is a way to have the FM sidebands at a high frequency to get low amplitude noise, while the cavity accepts the sidebands in exactly the same manner as it accepts the carrier so as to reduce the FM to AM noise conversion. This can be accomplished by frequency modulating the input laser beam at exactly the splitting frequency of the cavity free-spectral-range (FSR). We then detect and demodulate the cavity-transmitted light at the modulation frequency. The small residual frequency variations of the laser will still lead to some amplitude fluctuations and small optical phase shifts of the transmitted carrier, but they will also lead to exactly the same amplitude fluctuations and phase shifts of the sidebands which are transmitted on adjacent or nearby cavity axial orders. So the transmitted light still accurately represents an FM spectral triplet, with minimal AM conversion due to the relative laser/cavity frequency jitter. Thus the noise level can approach the intrinsic AM noise level of the laser at the FSR frequency, typically a few hundred MHz or a few GHz.

Figure 1 shows the case where the central component is tuned to the intracavity molecular resonance. Initially all the FM components are lined up with their respective cavity modes. The central cavity mode will then be frequency pulled due to the additional phase shift by the molecular dispersion. The detector viewing the transmitted light will thus generate a dispersion signal in the rf beat after the phase sensitive demodulation. We can refer to this technique as (laser frequency-) Noise-Immune Cavity-Enhanced Optical Heterodyne Molecular Spectroscopy ("NICE-OHMS"). This modulation and detection scheme enables profitable use of the high cavity finesse without a noise penalty.
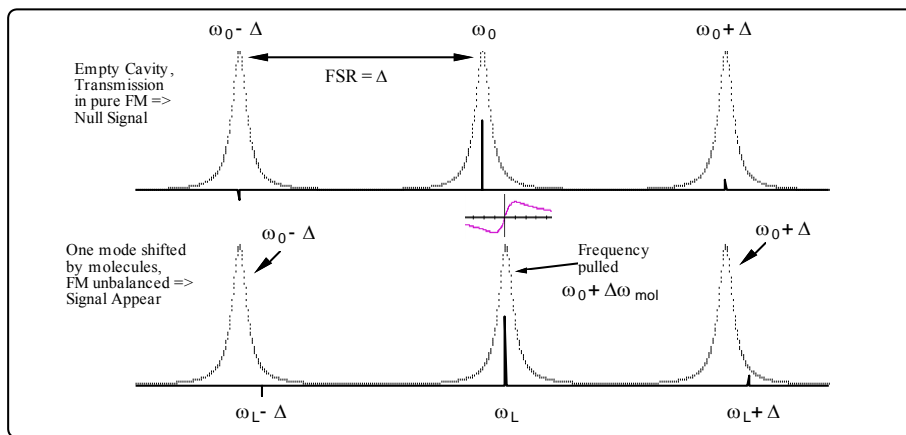

Fig.1 The optical spectrum and the detection principle for NICE-OHMS. FM symmetry is upset when molecular dispersion shifts a cavity resonance by $\Delta\omega_{mol}$. ω_L denotes the laser frequency.

To estimate the sensitivity associated with NICE-OHMS, we simply notice the cavity-enhancement effect applies only to the signal, with no additional noise. Therefore the sensitivity is simply that of Equation (2), divided by the cavity enhancement factor, namely (2 · Finesse/π). The power in the denominator should of course be that of the cavity transmitted light. This straightforward argument can be supplemented with a more rigorous proof. Suppose the molecular dispersion changes the intracavity refractive index by Δn, with the shift of cavity resonance given by ($\Delta n \cdot \omega_0$). Light going through the cavity will thus acquire an extra phase shift of $\phi = \arctan(\Delta n \cdot \omega_0 / \gamma)$, where γ is the cavity HWHM. Following the previous treatment and under the assumption of a small ϕ, we derive

$$\phi \approx \Delta n \cdot \omega_0 / \gamma = \frac{\lambda}{4\pi} \alpha \frac{\omega_0}{\gamma} = \frac{c}{2\gamma} \frac{\alpha L}{L} = \frac{FSR}{\gamma} \cdot (\alpha L) = \frac{2 \cdot Finesse}{\pi} \left(\frac{\alpha L}{2} \right),$$ (8)

which implies that

$$(\alpha L)_{min} = \frac{\pi}{2 \cdot Finesse} \left(\frac{2eB}{\eta P_t} \right)^{1/2} \frac{\sqrt{2}}{J_0(\beta)J_1(\beta)} .$$ (9)

A numerical example is given here to better serve the illustration. Suppose the modulation index $\beta = 0.5$ and the photodiode responsivity $\eta = 0.85$ Amps/Watt. Also assume the total optical power $P_t = 5$ mW and the detection bandwidth = $1/2\pi$ Hz, corresponding to a 1s time constant. Then for a single-pass cell, the noise-equivalent integrated absorption is: $(\alpha L)_{min} = 2.2 \times 10^{-8}$. Under the same conditions, a cavity with a finesse of 100,000 improves the sensitivity to: $(\alpha L)_{min} = 3.5 \times 10^{-13}$. We have indeed achieved a noise equivalent sensitivity of 5.2×10^{-13} of an integrated absorption at 1-s averaging, corresponding to an absorption of 1×10^{-14}/cm.

5. Experimental Setup and Sensitivity Results

The general experimental schematic is shown in Figure 2. One may use two electro-optic phase modulators to impose two sets of FM sidebands on the laser beam. The modulation at a low frequency δ is detected in the cavity reflection signal to produce the cavity dispersion locking error for stabilizing the laser onto the cavity. The sidebands at the high modulation frequency $\Delta = FSR$ are used to probe the intracavity molecular resonances and are detected in cavity transmission, after some adequate optical isolation between the cavity and the photodiode. To study the resonance signal lineshape and width, a precision scanning capability for the spectrometer is important. A frequency offset locking loop is implemented to permit sweeps with an rf resolution of the laser frequency relative to a stable reference. During the scan, the cavity FSR will change slightly. To maintain the noise-immune property, we actively track the sideband frequency to the cavity FSR value.

Fig.2 General schematic of the NICE-OHMS spectrometer, showing the major components of the laser/cavity locking, the transmitted sideband detection, and the precision tuning control.

We have to point out that although the requirement of the laser/cavity locking is much more relaxed for NICE-OHMS than in the direct cavity transmission detection, the laser linewidth still needs to be narrowed so that a stable optical power is effectively coupled into the cavity. For metrology purpose, this laser/cavity locking loop also serves as the short term frequency stabilizer. For a cavity linewidth of, say, 10 kHz, it is straightforward to lock a commercially available external-cavity diode laser below 100 Hz relative to the cavity, using a simple feedback control of the laser diode's current and the PZT of its external grating. In our experiment an all solid-state Nd:YAG laser was used. With the combined servo actions of the laser's internal piezo-electric transducer (PZT) and an external acousto-optic modulator (AOM), we obtained for laser/cavity locking a residual frequency noise spectral density of 20 mHz/√Hz. This indicates the laser's linewidth relative to the cavity is a mere 1.3 mHz.[15] Another important technical issue is that the recovered lineshape is influenced by a residual AM (RAM) associated with FM at the cavity FSR frequency. With an active control loop we are able to eliminate the RAM[16] at Δ and obtain a lineshape matching perfectly to a theoretical model, resulting in a flat and nearly shot-noise limited background for the fit residual throughout the entire tuning range of the resonance.

To obtain a further rejection of noise and baseline drift, we apply a small dither on the cavity resonance (with the modulation amplitude matching the width of molecular resonance) at a low audio frequency. This allows a lock-in to process the demodulated rf signal from the output of the double-balanced mixer which is driven at frequency Δ. Hence the final signal lineshape from the rf channel, resulting from modulation detection of an isolated dispersion resonance, approximates the derivative of dispersion.[17] Indeed the experimental data fit to the theoretical lineshape rather well, as shown in Figure 3, with the fit residual magnified by 10 times. Although the intrinsic transition width associated with the $(\nu_2+3\nu_3)$ P(5) line of C_2HD is on the order of kHz, the observed linewidth (FWHM) is 705 kHz (after removal of the modulation broadening by the fit) which includes contributions from the power- (saturation ~ 1.3x) and pressure-broadenings (~ 35 kHz/mTorr) of the 270 kHz transit time linewidth.

Fig.3 Frequency scan of the C_2HD $(\nu_2+3\nu_3)$ P(5) transition lineshape and overlaid theoretical fit, with fit residuals magnified by 10 times.

As explained earlier, one straightforward approach to probe the intracavity resonance is by dithering the locked laser/cavity system with a subsequent lock-in detection of the direct cavity transmission. We call this low-frequency operation a DC detection, in contrast to the high-frequency rf system used in the NICE-OHMS channel. The signal lineshape from this DC channel follows the original Wahlquist formula[18] of a modulation-broadened derivative of absorptive resonance. Comparison between the two detection channels, NICE-OHMS vs. DC, gives us true appreciation of the noise-immune nature of the NICE-OHMS detection. To have a clear demonstration, we deliberately set the laser/cavity lock to be loose and even oscillating, then we compare the recovered signal-to-noise ratios (S/N) before and after the lock was sabotaged. The result is shown in Figure 4. The DC detection of the intracavity molecular absorption (upper row) is shown to be critically dependent upon the performance of the laser/cavity lock. (A fast laser/cavity frequency-lock servo was used for the graphs obtained in the left column while a slow and noisy servo was used for those in the right column.) However, increased laser frequency noise (relative to the cavity) yields little effect in our FM detection (bottom row).

Figure 5 shows the experimental sensitivity we have achieved using 1.8 mTorr C_2HD gas. The cavity finesse is 100,000 and the intracavity buildup power is ~ 300 W, giving a saturation parameter of ~ 1.75 and a saturation peak contrast of 13.2%. The single-pass (46.9 cm long cavity) linear absorption is about 3×10^{-8}. Therefore the absolute level of saturated absorption by the intracavity molecules is 4×10^{-9}. This is verified by the DC detection of the cavity transmission, shown in the top graph of the figure. The calibration process involves measurement of cavity finesse, on-resonance transmission, and reflection dip contrast, from which we calculate the residual round-trip cavity losses. With the laser locked tightly onto the cavity with a relative linewidth of ~ 1 milliHertz, the simple cavity-dither and lock-in detection of the transmission yields a S/N (amplitude/rms noise) of 130 at 1-s averaging. This corresponds to a detection sensitivity of 3×10^{-11} at 1 s. The corresponding S/N from the NICE-OHMS detection is 7700 with a 1 s time constant, as shown in the bottom graph of the figure. This translates into a noise-equivalent detection sensitivity of 5.2×10^{-13} at 1 s averaging, about 1.5 times worse than the shot noise limit calculated previously. The NICE-OHMS result is ~ 60 times better than the straightforward dither detection, basically because of its higher modulation frequency (319 MHz FM sideband frequency compared with 500 Hz dither frequency) and its insensitivity towards the laser frequency noise relative to the cavity.

There exists an optimum value of the intracavity sample pressure for the maximum signal size. An increase of pressure raises the size of linear absorption, but at the same time reduces the level of saturation due to the pressure-broadening of the homogeneous transition width. For fixed cavity parameters, change of pressure also influences the input power coupling. We typically find the optimum pressure around 10 mTorr for the maximum saturation signal size.

Fig.4 Demonstration of the noise-immune property of NICE-OHMS. The C_2HD ($\nu_2 + 3\nu_3$) P(5) resonance signal is recovered by both cavity-dither lock-in (DC) detection and NICE-OHMS technique, under the conditions of a tight laser/cavity lock (left column) and a substantially deteriorated lock (right column).

Fig.5 Sensitivity measurement of the NICE-OHMS technique. The upper graph shows the level of the saturated absorption while the lower graph shows the corresponding S/N obtained via NICE-OHMS. The noise equivalent detection sensitivities (normalized to 1s time constant) are 3×10^{-11} for cavity dither detection and 5.2×10^{-13} for NICE-OHMS.

The high detection sensitivity, now increased by 5 orders of magnitude by the use of NICE-OHMS method, really opens up many new possible spectroscopic applications. As an example, we have recovered some other weaker transitions within the tuning range of the Nd:YAG laser at 1.064 μm. We have measured two such lines, namely $^{12}C_2H_2$ ($2\nu_1 + \nu_2 + \nu_5$) R(12)[19] and $^{12}C^{16}O_2$ ($2\nu_1 + 3\nu_3$) R(6),[20] with their respective transition dipole moment of 50 μDebye and 6 μDebye. (1 Debye = 3.33564×10^{-30} C·m) They are both weaker than the C_2HD ($\nu_2 + 3\nu_3$) P(5) transition, which has a transition dipole moment of ~ 70 μDebye. Using the same gas pressure, optical power, and cavity dither amplitude, we compare the saturated absorption signals of CO_2, C_2HD and C_2H_2 in Figure 6. The C_2H_2 transition is recovered with an excellent signal-to-noise ratio, as shown in Figure 6 (c). The signal size is about 0.23 of that for C_2HD, using the same gas pressure and optical power. It provides another frequency reference for the Nd:YAG laser.

For the CO_2 transition, however, the saturated absorption signal is much weaker than the C_2HD line, by more than a factor of 350. This CO_2 resonance involves two quanta of symmetric stretch and three quanta of antisymmetric stretch of the C-O bond. The bending mode (ν_2) is not excited. The lifetime of the excited vibrational state is estimated to be ~ 2 ms, mainly due to the ir fluorescence on the vibrational transition $(2, 0^0, 3) \prod (2, 0^0, 2)$. The relevant molecular constants are in Ref. 21. Under exactly the same experimental conditions (except for the change of sample gas), the recovered lineshape associated with the $^{12}C^{16}O_2$ ($2\nu_1 + 3\nu_3$) R(6) transition is vastly different from either C_2HD or C_2H_2, as indicated in Figure 6. In fact, our theoretical model for the nearly perfect fit of the experimental data involves two separate resonances that have

different linecenters and linewidths. More importantly, the narrower negative-going peak indicates a physical process reversed from the normal saturated absorption. The intracavity optical power is 410 W, where the saturation of this CO_2 transition is estimated to be only a few percent (2%) in the free-flight regime. As we reduce the input power by a factor of 4, the resonance lineshape remains relatively unchanged. The signal size, however, reduces roughly by the square of the power change. The lineshape does not depend upon the laser dither frequency either. The change of the dither amplitude, on the other hand, will surely have a larger impact on the signal size of the relatively wider peak, thereby causing the apparent change on the signal lineshape. This change is well accounted for by our theoretical model and our fit is able to produce basically consistent linewidths corresponding to a certain gas pressure.
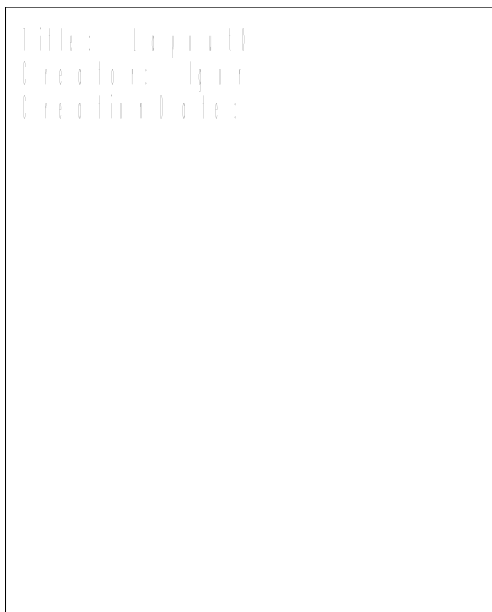

Fig.6   Lineshape comparison among the resonances of (a) CO_2, (b) C_2HD, and (c) C_2H_2, under the same experimental conditions.

As we change the intracavity gas pressure, we witness linewidth broadenings and linecenter shifts for both peaks. Extrapolated to zero pressure, the inverted peak has a FWHM of ~ 100 kHz. One likely explanation for the abnormal lineshape is the existence of a near-resonant two-photon transition in the neighborhood of the one-photon resonance. This is supported by the fact that the zero-pressure linewidth of the inverted peak is only about 100 kHz, half of that dictated by the transit time broadening (210 kHz). It is as if during the transit, the molecule experiences twice as many radians of signal phase, for example by resonating with a two-photon response. A second possible physical effect is the existence of some quantum interference due to the state mixing of the excited vibrational state.

6. Application to Laser Frequency Stabilization

In the work of optical frequency metrology, NICE-OHMS technique can provide us with thousands of weak molecular lines as high quality visible frequency/wavelength references. The narrow linewidths associated with these molecular transitions are invaluable, as they make better definitions of the linecenters to enable long-term stabilities. The high signal-to-noise ratio of the resonance information helps to reach the desired short-term stability in reduced averaging time, permitting more effective intercomparisons among various frequency standards. With the narrower linewidth - but lower S/N - of the C_2HD overtone transition, we have currently achieved a level of stability similar to that of the I_2 system.[22] However, the long natural lifetime of overtone transitions offers the opportunity for optical selection of slow molecules to produce a much narrower linewidth than the room temperature transit time limit. This should further improve the long term stability and reproducibility.

The NICE-OHMS spectrometer provides laser frequency discrimination information separately relative to both the cavity resonance and the molecular transition. It is thus an ideal system to achieve simultaneously good short- and long-term frequency stabilizations. As discussed earlier, the laser basically tracks the cavity resonance on the precision level of a few milliHertz. The cavity's vibration noise and its long-term drift can be suppressed by stabilizing to the intracavity molecular resonance. The NICE-OHMS signal is intrinsically dispersive when the molecular resonance is probed by the carrier of the FM triplet. Used optimally for locking, this could basically eliminate the influence of the local oscillator frequency drift on

the recovered linecenter. In practice we found it necessary to dither additionally the cavity length and make a 2nd harmonic signal recovery of the rf mixer output. This is to partly suppress the baseline offset problem associated with the imperfect FM modulation at the FSR frequency. Figure 7 shows such a discrimination curve associated with the C_2HD transition. Another important issue concerns the final lineshape under the conditions of FM with a residual AM part (RAM). RAM simply adds an even-symmetric absorption-phase component to the originally pure dispersion. Unfortunately, this lineshape alteration caused by RAM cannot be corrected by the cavity-dither process. To achieve the best stabilization results, it is crucial that the FM has a zero (or at least a small constant) residual AM. Active control of the FM modulator was used in our current setup.[16]

Fig.7 Molecular discrimination signal used for stabilizing Nd:YAG laser, obtained by the 2nd derivative recovery of the dispersion signal detected by NICE-OHMS.

We checked the quality of this overtone-stabilized laser at 1.064 μm against a frequency-doubled Nd:YAG/I_2 reference system[22] via optical heterodyne beat. (The 532 nm-stabilized laser has a stability ~5 x10^{-14} at 1 s, from beating experiments with two I_2-stabilized systems.) In Figure 8 the counted beat frequency vs. time shows a drift ~ 5 Hz/h and a 60 Hz frequency noise at 1-s counter gate time, in direct agreement with the S/N available at 1.064 μm. The reference Nd:YAG laser (after frequency doubling) is locked on I_2: R(56) 32-0, component a_{10}.[22] With the mean value of the beat frequency between the two lasers at 5252.2261 ±0.0026 MHz, we determine the absolute frequency of the P(5) line in the ($v_2 + 3\ v_3$) band of $^{12}C_2HD$ to be 281,635,363.962 MHz ± 20.2 kHz. The 20 kHz uncertainty is almost entirely due to the limited knowledge of the absolute frequency of the Nd:YAG/I_2, our secondary standard. Similarly, the center frequency of the $^{12}C_2H_2$ ($2v_1 + v_2 + v_5$) R(12) line is determined to be 281,612,403.278 (.025) MHz, i.e., it is 17708.458 (.014) MHz red of the iodine-locked reference laser.

Fig.8 Stability of beat between I_2-stabilized and C_2HD-stabilized Nd:YAG lasers. Allan variance is calculated from the beat record. The frequency noise of the beat is still limited by the C_2HD system, which is ~ 3 times worse than the I_2 system.

A very effective representation of the frequency noise in the time domain is by the Allan variance.[23] In calculating the Allan variance one simply compares adjacent frequency measurements and then averages over the whole data set. The time interval between the adjacent measurements is basically the averaging time for the frequency noise. The Allan variance permits one to separate and isolate different noise processes based on their time scales. In the short-time domain, the Allan variance typically displays a slope of $\tau^{-1/2}$, where τ is the averaging time. This is because the main contribution to the fast noise originates from white noise, for example, shot noise. One sees immediately from this argument that the level of this short-term variance is fixed by the ratio between the frequency discrimination linewidth and its S/N. Figure 8 also shows the calculated Allan variance from the beat record of the two stabilized lasers. The variance is normalized to the optical carrier frequency, i.e., 282 THz (1.064 μm). The Allan variance of $\sigma_y = 2$ x $10^{-13}/\sqrt{\tau}$ improves to 6 x10^{-15} at a longer integration

time (> 1000 seconds), a promising indicator for an ultrastable frequency reference. This amazing frequency stability achieved by the extremely weak reference transition is a direct result of our spectrometer's ultra-high detection sensitivity. Notice that the C_2HD-stabilized system shows only 3 times more noise than the I_2 system, a remarkable success considering the green I_2 transition strength is almost a million times stronger than the P(5) line of the C_2HD ($\nu_2 + 3 \nu_3$) overtone band. The short-term frequency stability of the optical sources are comparable to or better than the state-of-the-art microwave standards. However, the optical reproducibility and accuracy are not yet comparable. The urgent task is therefore to vastly reduce the systematic influences on the apparent line-centers of optical transitions.

One important aspect of reducing the systematic shift of the reference frequency is to slow down the motion of the target quantum absorber, thereby reducing the 2nd order Doppler effect. Slow speed also implies longer interaction time. Slower molecules correspond directly to narrower linewidth since the natural life-time of vibration transitions usually far exceeds (more than 300 times in our case) the interaction time limited by general laboratory laser field dimensions. Lacking an effective scheme for molecular cooling and trapping, optical selection of slow molecules based on interaction time has been actively pursued.[24,25,26] The homogeneous linewidth originating from the collisional broadening can be reduced by lowering the gas pressure, until the mean-free-path of molecules gets much larger than the transverse field dimension, thereby creating the so-called transit-time regime. To optically select the slow molecules, low optical power is necessary so that the low Rabi frequency leads to appreciable saturation only for the slowest molecules. This limits the final contribution to the signal only by slow molecules and consequently the effective interaction time and the instrumental resolution are increased.

In the free-flight regime, molecules with the mean thermal velocity cross the laser beam without suffering any collision. In other words, if we define the collision-broadened homogeneous linewidth (HWHM) as Γ_p and the transit-time linewidth as Γ_t, then $\Gamma_p << \Gamma_t$, with $\Gamma_t = (\pi/4) <V_\perp>/w_0$, where w_0 is the laser beam-waist radius and $<V_\perp>$ is the mean transverse velocity. A second important time scale is the inverse of the collisional linewidth Γ_p. Slow molecules are those with transit time longer than $1/\Gamma_p$. They spend their whole life-time inside the field and are still in a collisional regime. They have a constant and velocity-independent saturation parameter S, controlled primarily by the collisional broadening,

$$S = \frac{\mu^2 E^2}{\hbar^2 \Gamma_p^2} \ , \tag{10}$$

where μ is the transition dipole moment and E is the optical field amplitude. Fast molecules with transit time shorter than $1/\Gamma_p$ are in a free-flight regime and their saturation parameter depends on their transverse velocity. If we define τ as the interaction time which is on the order of $\tau \approx 4w_0/V_\perp$, then S equals to unity when $(\mu E/\hbar)\tau = \pi$. The optical power required to saturate molecules with transverse velocity $V_\perp$ is thus

$$Power_{(S=1)} = \left(\frac{c\varepsilon_0}{2} E^2\right) \pi w_0^2 /2 = \frac{c\varepsilon_0}{2} \left(\frac{\pi\hbar}{\mu} \frac{V_\perp}{4w_0}\right)^2 \frac{\pi w_0^2}{2} = \frac{\pi^3}{64} \frac{\hbar^2 c\varepsilon_0}{\mu^2} V_\perp^2 \ . \tag{11}$$

The necessary saturation power increases as the square of the transverse velocity, and it can be vastly different for slow and average thermal molecules since we have assumed that $\Gamma_p << \Gamma_t$. In short, a sufficiently low gas pressure can be used to create a free-flight regime, and a low power beam then optically selects the slow molecules. The selection is based on the saturation effect. The resulting signal linewidth becomes strongly inhomogeneous, with molecules from different transverse velocity groups contributing different intensities and widths. Slow molecules will dominate the contribution to the signal amplitude, and the width is essentially the homogeneous linewidth Γ_p. Faster moving molecules will see a reduced saturation and will mostly contribute to the wings of the resonance. The width is caused by transit effects and increases with velocity.

In experiment we used < 2 mTorr sample gas, and the mean-free-path of molecules is ~ 30 times longer than the transverse field dimension. The cavity input power is reduced 75 times from normal operation. Figure 9 shows a resonance linewidth of ~ 20 kHz, without correction for the modulation broadening by a 30 kHz peak-to-peak dither of the cavity. This is thirteen times narrower than that set by the room temperature transit-time-limit and is mainly limited by the relatively high pressure (1.8 mTorr). The selected molecules have a temperature of ~ 1.8 Kelvin. The signal-to-noise ratio is vastly reduced, as the optical power is much smaller than usual and the majority of molecules do not contribute to the observed saturation signal. In fact, compared with the number of molecules participated in the normal saturation spectroscopy, the slow molecule selection process has reduced that number to only a fraction of 0.75%. At present the limited S/N associated with the low power has prevented us from taking full advantage of this narrow linewidth. With an improved system this approach will enable us to access the information of free molecules with minimized second order Doppler shift, thereby creating an optical frequency standard of potentially high accuracy.

Fig.9 With low power and gas pressure, optical selection of slow molecules produces a linewidth 13 times below the room-temperature transit-time-limit.

7. Conclusions and Acknowledgment

The demonstration of the sensitivity level of 5.2 x 10^{-13} integrated absorption has certainly established NICE-OHMS among the most sensitive detection methods currently available. The principle is simple, using an external cavity to boost the signal contrast with a fast modulation/recovery scheme to eliminate technical noises associated with the laser and the cavity. While this unprecedented sensitivity will be surely enjoyed by many other applications, it has already shown a tremendous capability to advance the field of optical frequency metrology.

† Present address: Quantum Optics Group, California Institute of Technology, Pasadena, CA.
☞ Permanent address: Department of Physics, East China Normal University, Shanghai, China.
‡ Staff member, Quantum Physics Division, National Institute of Standards and Technology, Boulder, CO.

8. Reference

1. J. L. Hall, L. Hollberg, L.-S. Ma, T. Baer and H. G. Robinson, J. Physique-Colloque **42**, suppl. 12, C8 59-71 (1981).
2. G. C. Bjorklund, Opt. Lett. **5**, 15-17 (1980).
3. J. L. Hall, L. Hollberg, T. Baer, and H. G. Robinson, Appl. Phys. Lett. **39**, 680-682 (1981).
4. T. W. Hänsch, A. L. Schawlow and P. E. Toschek, IEEE J. Quan. Electron. **QE-8**, 802 (1972).
5. H. J. Kimble, IEEE J. Quan. Electron. **QE-16**, 455 (1980).
6. T. D. Harris, in "Ultrasensitive Laser Spectroscopy," 343, D. S. Kliger, ed., Academic Press, New York (1983).
7. J. Altmann, R. Baumgart and C. Weitkamp, Appl. Opt. **20**, 995 (1981).
8. A. Kastler, Appl. Opt. **1**, 17 (1962).
9. P. Cerez, A. Brillet, C. N. Man-Pichot and R. Felder, IEEE Trans. Instrum. & Meas. **29**, 352 (1980).
10. L-S. Ma and J. L. Hall, IEEE J. Quan. Electron. **QE-26**, 2006 (1990).
11. M. De Labachelerie, K. Nakagawa and M. Ohtsu, Opt. Lett. **19**, 840 (1994).
12. A. O'Keefe and D. A. G. Deacon, Rev. Sci. Instrum. **59**, 2544 (1988).
13. J. L. Hall and C. J. Bordé, Appl. Phys. Lett. **29**, 788 (1976).
14. C. Wieman and T. W. Hänsch, Phys. Rev. Lett. **36**, 1170 (1976).
15. D. Hils and J. L. Hall, in "Frequency Standards and Metrology," Ed. A. De Marchi, Springer-Verlag, Berlin (1989).
16. J. L. Hall, J. Ye, L.-S. Ma, K. Vogel, and T. Dinneen, in *Laser Spectroscopy XIII*, Y. Z. Wang, Ed., World Scientific, in press (1997).
17. R. L. Smith, J. Opt. Soc. Am. **61**, 1015 (1971).
18. H. Wahlquist, J. Chem. Phys. **35**, 1708 (1961).
19. K. Nakagawa, T. Katsuda, A. S. Shelkovnikov, M. de Labachelerie, and M. Ohtsu, Opt. Commun. **107**, 369-372 (1994).
20. P. Fritschel and R. Weiss, Appl. Opt. **31**, 1910-1912 (1992).
21. L. S. Rothman and L. D. G. Young, J. Quant. Spectrosc. Radiat. Transfer **25**, 505-524 (1981).
22. P. Jungner, M. Eickhoff, S. Swartz, J. Ye, J. L. Hall and S. Waltman, SPIE **2378**, 22, (1995).
23. D. W. Allan, Proc. IEEE **54**, 221 (1966).
24. Ch. J. Bordé, J. L. Hall, C.V. Kunasz and D. G. Hummer, Phys. Rev. **14**, 236 (1976).
25. S. N. Bagayev, V. P. Chebotayev, A. K. Dmitriyev, A. E. Om, Yu. V. Nekrasov, and B. N. Skvortsov, Appl. Phys. B **52**, 63 (1991).
26. Ch. Chardonnet, F. Guernet, G. Charton, and Ch. J. Bordé, Appl. Phys. B **59**, 333 (1994).